

Concept-TRAK: Understanding how diffusion models learn concepts through concept-level attribution

Yonghyun Park^{1*}
Naoki Murata¹

Chieh-Hsin Lai¹
Wei-Hsiang Liao¹
Junghyun Koo¹

Satoshi Hayakawa²
Woosung Choi¹
Yuki Mitsufuji^{1,2}

Yuhta Takida¹
Kin Wai Cheuk¹

SONY AI¹ Sony Group Corporation²

Abstract

While diffusion models excel at image generation, their growing adoption raises critical concerns around copyright issues and model transparency. Existing attribution methods identify training examples influencing an entire image, but fall short in isolating contributions to specific elements, such as styles or objects, that matter most to stakeholders. To bridge this gap, we introduce *concept-level attribution* via a novel method called *Concept-TRAK*. Concept-TRAK extends influence functions with two key innovations: (1) a reformulated diffusion training loss based on diffusion posterior sampling, enabling robust, sample-specific attribution; and (2) a concept-aware reward function that emphasizes semantic relevance. We evaluate Concept-TRAK on the AbC benchmark, showing substantial improvements over prior methods. Through diverse case studies—ranging from identifying IP-protected and unsafe content to analyzing prompt engineering and compositional learning—we demonstrate how concept-level attribution yields actionable insights for responsible generative AI development and governance.

1 Introduction

Data attribution methods [22, 29, 14], which estimate how much each training example contributes to a generated output, have become valuable tools for tasks such as data valuation [20], curation [26] and understanding model behavior [35]. The impressive success of large-scale diffusion models [38, 42, 17] in image generation, often coupled with substantial commercial impact [31, 10, 34], has been largely driven by access to massive training datasets [36]. However, this dependence raises pressing societal concerns, especially around copyright and data ownership [50, 40, 5, 39, 13, 4]. A key question is whether generated outputs can be traced back to specific training samples, enabling the detection of copyrighted content used during training—an area where data attribution methods show significant promise [9].

While recent work has begun exploring attribution methods tailored for diffusion models [52, 23, 27, 48], these approaches generally estimate contributions at the level of entire images. This broad perspective poses a critical limitation: in many practical scenarios, stakeholders care about specific concepts within an image, rather than the whole composition.

For example, consider an AI-generated image depicting an IP-protected character (e.g., Pikachu) rendered in a pencil drawing style as shown in Figure 1(a). In such cases, copyright concerns from IP holders (e.g., The Pokémon Company) would primarily focus on the character itself, not the stylistic pencil rendering. Yet, traditional attribution methods—such as TRAK—identify training samples that influenced the generation of the full image, failing to isolate those tied to particular

*Work done during an internship at SONY AI. Email: park19@seas.upenn.edu

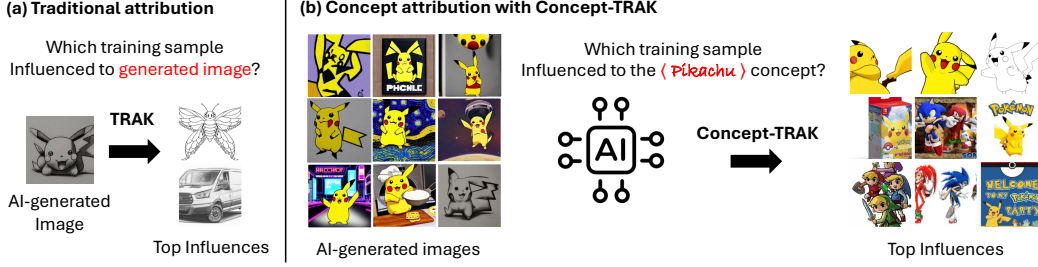


Figure 1: (a) Traditional attribution methods like TRAK identify training samples that influenced an entire generated image, often yielding influences unrelated to specific concepts of interest. (b) Our *Concept-TRAK* identifies training samples that specifically influenced a targeted concept (e.g., "Pikachu"), enabling precise attribution for features of interest.

concepts. As Figure 1(a) demonstrates, these methods tend to retrieve stylistically similar images (e.g., pencil-drawn moths or vehicles) but miss the character that is actually subject to copyright protection.

To address this, we introduce the notion of **concept-level attribution**, which estimates each training example’s contribution to specific semantic features such as styles, objects, or concepts. Building on this, we propose *Concept-TRAK*, an extension of influence functions [22], to quantify how training data affects the model’s output probabilities for *individual concepts*. *Concept-TRAK* incorporates two key innovations: (1) a reformulated diffusion training loss based on diffusion posterior sampling (DPS), yielding robust, sample-specific attribution gradients; and (2) a concept-aware reward function that emphasizes semantic relevance. These components significantly enhance attribution fidelity. As shown in Figure 1(b), *Concept-TRAK* correctly identifies training samples responsible for the concept of *Pikachu*, rather than irrelevant stylistic cues—enabling precise, interpretable, and stakeholder-relevant attribution for tasks such as copyright auditing and model transparency.

To rigorously evaluate our method, we adopt a retrieval-based benchmark, AbC benchmark [47], for concept attribution. In this setting, *Concept-TRAK* significantly outperforms prior methods by accurately retrieving training examples that influence specific concepts. Moreover, we demonstrate its practical value through case studies that: (1) identify training samples that contributed most to learning IP-protected concepts, (2) detect the sources of learning unsafe concepts, (3) trace the origins of both desirable features and problematic outputs for model debugging, and (4) provide insights into the origins of relational knowledge (e.g., shake hands, hugs) in diffusion models. Together, these results highlight how concept-level attribution offers valuable insights both for practical applications and for advancing our understanding of how generative models learn and combine concepts from training data.

2 Background

2.1 Diffusion Model

Diffusion models [38, 42, 17] are a class of generative models that synthesize images through an iterative denoising process. Starting from a clean image x_0 , the forward process adds Gaussian noise to produce a sequence of increasingly noisy images x_t , following, $q(x_t | x_0) = \mathcal{N}(\sqrt{\alpha_t}x_0, (1-\alpha_t)I)$, where α_t is a noise schedule controlling the level of corruption at timestep t .

A neural network $\epsilon_\theta(x_t, t)$ is trained to predict the added noise ϵ , enabling reconstruction of x_0 from x_t at noise level t . The training objective is called the denoising score matching (DSM) loss: $\mathcal{L}_{\text{DSM}}(x_0; \theta) = \mathbb{E}_{x_0, t, \epsilon} [\|\epsilon - \epsilon_\theta(x_t, t)\|_2^2]$, which encourages the model to approximate the gradient of the log-density (i.e., score function): $\epsilon_\theta(x_t, t) \propto \nabla \log p_t(x_t)$.

Diffusion models can be extended to conditional generation by incorporating additional information c , such as a text prompt [16, 28]. In this setting, the model learns $\epsilon_\theta(x_t, t; c) \propto \nabla \log p_t(x_t | c)$, allowing it to generate images that are not only realistic but also aligned with the conditioning input.

2.2 Data Attribution

The goal of data attribution is to estimate the contribution of a training sample x^i to a model’s utility loss \mathcal{V} —a performance metric or objective function that quantifies how well the model performs (e.g., test loss) [22, 29, 14]. A straightforward approach is the Leave-One-Out method, which involves removing a training example x^i , retraining the model, and measuring the change in performance. However, this naive strategy is computationally expensive for modern models and large-scale datasets, as it requires retraining the model once for every training point, making it practically infeasible.

To address this limitation, influence functions [22] efficiently approximate the effect of removing a training example x^i by using gradient-based estimates, avoiding the need for retraining. Given a model with parameters $\theta \in \mathbb{R}^d$ and training loss $\mathcal{L}(\cdot; \theta)$, the influence function is defined as:

$$\mathcal{I}(x^i, \mathcal{V}) \triangleq g_{\mathcal{V}}^{\top} \mathbf{H}^{-1} g_i.$$

Here, $g_i = \nabla_{\theta} \mathcal{L}(x^i; \theta)$ represents the gradient of the loss with respect to parameters θ for sample x^i , $g_{\mathcal{V}} = \nabla_{\theta} \mathcal{V}(\theta)$ is the gradient of utility function \mathcal{V} , and $\mathbf{H} = \nabla_{\theta}^2 \mathcal{L}(D; \theta)$ denotes the Hessian matrix of the training loss computed over the entire training dataset $D = \{x^i\}_{i=1}^N$. Intuitively, $\mathbf{H}^{-1} g_i$ corresponds to the parameter update that would result from one Newton step on x^i , and the inner product with $g_{\mathcal{V}}$ provides a first-order Taylor approximation of how this update would affect the model’s utility.

Due to the high cost of computing the full Hessian, influence function methods typically rely on inverse Hessian-vector products or approximations such as low-rank factorizations (e.g., EK-FAC) [15]. Despite these advances, influence functions remain challenging to apply in practice. Identifying training samples that strongly impact a target utility [6] requires computing gradients for every sample—an effort equivalent to a full training epoch. Unless these gradients are precomputed and stored, each attribution query results in prohibitive computational cost—especially for today’s large-scale pretrained models trained on massive datasets at great expense. Moreover, storing the full gradient for every training sample is infeasible, since each gradient matches the dimensionality of the model parameters.

To address this, TRAK [29] proposes projecting the gradients into a lower-dimensional space using a random projection matrix $P \in \mathbb{R}^{d \times k}$ with $k \ll d$, and then computing influence in the projected space:

$$\mathcal{I}(x^i, \mathcal{V}) \triangleq (P^{\top} g_{\mathcal{V}})^{\top} \mathbf{H}_P^{-1} P^{\top} g_i,$$

where $\mathbf{H}_P = P \mathbf{H} P^{\top} \in \mathbb{R}^{k \times k}$ is the projected Hessian. Since the projected dimensionality k is typically orders of magnitude smaller than the original model size d (e.g., $d/k \approx 10,000$), training gradients can now be stored on disk. When performing data attribution for a new utility, these stored projections can be efficiently reused without costly recomputation.

2.3 Data attribution for diffusion models

Prior work on diffusion models [51, 52, 23] has primarily focused on whole-image attribution, typically using the same objective for both training and utility losses. These studies reveal that attribution performance is highly sensitive to the choice of loss function. In particular, the standard DSM loss introduces stochasticity via both the noise term ϵ and the perturbed input x_t , resulting in noisy gradient estimates that require extensive averaging to be reliable—making it suboptimal for attribution. To mitigate this, D-TRAK [52] employs the squared ℓ_2 -norm $\|\epsilon_{\theta}\|_2^2$ to compute influence scores, achieving improved stability and accuracy. However, D-TRAK does not correspond to a proper learning objective tailored to a specific sample x_0^i . Consequently, the resulting gradients may fail to faithfully capture the unique contribution of x_0^i to the model’s learned behavior.

These findings highlight that **choosing a robust loss function for gradient computation is essential for reliable attribution in diffusion models**. We extend this insight to the concept-level setting, which demands loss functions specifically designed to capture concept-specific influence.

3 Method

We present *Concept-TRAK*, a framework for quantifying the contribution of individual training samples to specific concepts learned by diffusion models. Unlike prior work that relies solely on

high-variance per-sample training gradients for influence functions, our approach enables a more accurate estimation of both the training gradients and the gradients of a reward-based utility function that measures concept presence. This section details the proposed objective functions used to compute these key gradients.

3.1 Train Gradients: DPS-Loss

To address the challenges associated with the stochasticity of the DSM loss and the absence of sample-specific attribution for x_0^i , as discussed in Section 2.3, we introduce a novel training objective grounded in the principles of diffusion posterior sampling (DPS) [7], denoted by \mathcal{L}_{DPS} . This objective produces sample-specific training gradients without relying on a fully stochastic regression target and is explicitly designed to capture the influence of upweighting an individual sample x_0^i on the model’s output.

Intuition and Formulation. Consider the effect of finetuning a pretrained diffusion model ϵ_θ on a single sample x_0^i . To model this process, we adopt a generalized Bayesian update with power likelihood where the influence of x_0^i is amplified through multiplicative weighting [18] (Appendix B):

$$\tilde{p}(x) \propto p(x) \cdot p(x_0^i | x)^w,$$

where w is a weighting parameter. For attribution, we want to capture precisely how this upweighting affects the model’s behavior. In other words, the training loss for sample x_0^i can be conceptualized as learning to model the distribution $\tilde{p}(x)$.

Instead of directly training on x_0^i , could we learn to model $\tilde{p}(x)$? One approach would be to use explicit score matching (ESM) [43]. If we had access to a diffusion model $\tilde{\epsilon}$ that already trained on $\tilde{p}(x)$, we could replace DSM with ESM for model training [19]:

$$\mathcal{L}_{\text{ESM}}(x_0; \theta) := \mathbb{E}_{x_0, t} [\|\tilde{\epsilon}(x_t, t) - \epsilon_\theta(x_t, t)\|^2]. \quad (1)$$

A key advantage of ESM is its reduced reliance on the Monte Carlo-estimated regression target used in the DSM loss for influence function computation, resulting in more robust gradient estimates. Moreover, as we will show, $\tilde{\epsilon}$ can incorporate x_0^i as guidance information—unlike prior approaches [52]. However, directly obtaining $\tilde{\epsilon}$ would require expensive retraining for each sample x_0^i , which is impractical. To address this, we introduce an efficient, feasible, and robust approximation to $\tilde{\epsilon}$.

DPS Approximation. The core idea of our method is to approximate $\tilde{\epsilon}$ without additional training by using diffusion posterior sampling (DPS) principles [7]. For our target distribution $\tilde{p}(x) \propto p(x) \cdot p(x_0^i | x)^w$, the score function at timestep t becomes:

$$\nabla \log p_t(x_t) + w \cdot \nabla \log p_t(x_0^i | x_t).$$

The challenge lies in computing $\nabla_{x_t} \log p_t(x_0^i | x_t)$, which is not directly accessible. To approximate this term, we start from assuming the data distribution follows a mixture of Gaussians where $p(x_0^i | x_0) \propto \exp(-\|x_0 - x_0^i\|_2^2)$. Since this distribution is defined over clean images x_0 , we use the predicted clean image $\hat{x}_0^i = \mathbb{E}[x_0 | x_t]$ as a proxy

$$\log p_t(x_0^i | x_t) \approx \log p_t(x_0^i | \hat{x}_0^i) \propto -\|x_0^i - \hat{x}_0^i\|^2.$$

Taking the gradient and incorporating it into our score function yields:

$$\tilde{\epsilon}(x_t, t, x_0^i) = \epsilon_\theta(x_t, t) + \sqrt{1 - \bar{\alpha}_t} \cdot w \cdot \nabla_{x_t} \|x_0^i - \hat{x}_0^i\|^2.$$

Our final DPS-guided objective combines this with the ESM loss:

$$\mathcal{L}_{\text{DPS}}(x_t; \theta) = \|\text{sg}[\epsilon_\theta(x_t, t) + \underbrace{\sqrt{1 - \bar{\alpha}_t} \cdot w \cdot \nabla_{x_t} \|x_0^i - \hat{x}_0^i\|^2}_{\text{DPS guidance}}] - \epsilon_\theta(x_t, t)\|_2^2,$$

where $\text{sg}[\cdot]$ denotes stop-gradient. For clarity, we use a slight abuse of notation and denote $\mathcal{L}(x_t, \theta)$ as the loss at a single timestep t .

3.2 Utility Gradient: Reward-DPS-Loss

Having established how to compute training gradients, we now turn to the utility gradient needed for influence functions. For concept-level attribution, our utility function must capture the presence of specific concepts in generated images, rather than just whole-image probability or quality.

We formulate this as a reward-based approach, where a reward signal quantifies how much a concept (e.g., IP-protected contents or “smiling”) appears in a generated image. While various reward-based training losses exist in the literature, we propose a novel loss function based on our established DPS framework to ensure consistency between training and utility gradients. The gradient of this reward-based loss with respect to model parameters then serves as our utility gradient for influence computation.

Specifically, we leverage the insight that training a model with a reward function $R(x)$ modifies the learned distribution to $\tilde{p}(x) = \frac{1}{Z} p(x) \exp(\frac{1}{\beta} R(x))$, where Z is a normalizing constant and β controls the KL-divergence between p and \tilde{p} [33]. For this distribution, the score function at timestep t becomes:

$$\nabla \log p_t(x_t) + 1/\beta \cdot \nabla_{x_t} R(x_t).$$

By plugging this result into the ESM loss (Eq. 1), we obtain our final Reward-DPS-guided objective:

$$\mathcal{L}_{\text{Reward-DPS}}(x_t; \theta) = \|\text{sg}[\epsilon_\theta(x_t, t) - \underbrace{1/\beta \cdot \nabla_{x_t} R(x_t)}_{\text{Reward guidance}}] - \epsilon_\theta(x_t, t)\|_2^2,$$

where $\text{sg}[\cdot]$ denotes stop-gradient.

It is worth noting the mathematical relationship between our training loss and utility function formulations. By setting $\frac{1}{\beta} R(x_t) = w \log p_t(x_0^i | x_t)$, the Reward-DPS framework directly generalizes our earlier DPS approach. In this special case, the reward function quantifies the log-likelihood of the noisy latent x_t given the training sample x_0^i , which we previously approximated as proportional to $-\|x_i^0 - \hat{x}_i^0\|^2$. This unifying perspective demonstrates that both our training loss and utility function derive from the same mathematical foundation, ensuring theoretical consistency in our gradient computations.

We focus on measuring utility gradients for textual concepts. Extensions to other reward types, including implicit rewards [33], explicit reward models, and rewards for local concept attribution, are discussed in Appendix C.

Textual Concepts. For textual concepts, we model the reward using conditional probabilities: $R(x_t) \propto \log p_t(c | x_t)$. The gradient of this reward becomes $\nabla_{x_t} R(x_t) \propto \nabla_{x_t} \log p_t(x_t | c) - \nabla_{x_t} \log p_t(x_t)$, which directly corresponds to the classifier-free guidance [16].

To effectively isolate specific textual concepts, recent research [12, 49, 3, 24] demonstrates the importance of contrastive prompt engineering. Rather than using a single concept descriptor, defining concepts through comparison between positive and negative expressions yields more precise concept isolation. For example, attributing the concept “old” is more effective by comparing “old woman” to “young woman,” as this isolates age within a consistent context. Thus, we define our concept trio: c = “woman” (base), c^+ = “old woman” (positive), and c^- = “young woman” (negative), enabling attribution of “old” specifically within the context of the base noun.

This contrastive approach aligns naturally with our guidance-based framework, leading to the following Reward-DPS loss formulation:

$$\mathcal{L}_{\text{Slider}}(x_t; \theta) = \|\text{sg}[\epsilon_\theta(x_t, t; c) + \underbrace{1/\beta \cdot [\epsilon_\theta(x_t, t; c^+) - \epsilon_\theta(x_t, t; c^-)]}_{\text{Classifier-free guidance}}] - \epsilon_\theta(x_t, t; c)\|_2^2,$$

where $\epsilon_\theta(x_t, t; c)$ is the model’s prediction conditioned on prompt c .

Note that this loss is equivalent to the concept slider loss [12], which discovers concept directions in parameter space. Here, the guidance term $[\epsilon_\theta(x_t, t; c^+) - \epsilon_\theta(x_t, t; c^-)]$ corresponds to $-\nabla_{x_t} R(x_t)$ in our general formulation.

3.3 Additional Techniques for Enhancing Concept-Level Attribution

Deterministic Sampling via DDIM Inversion To eliminate stochasticity from the forward diffusion process $x_t \sim q(x_t | x_0)$, we employ deterministic DDIM inversion [41] to derive a deterministic

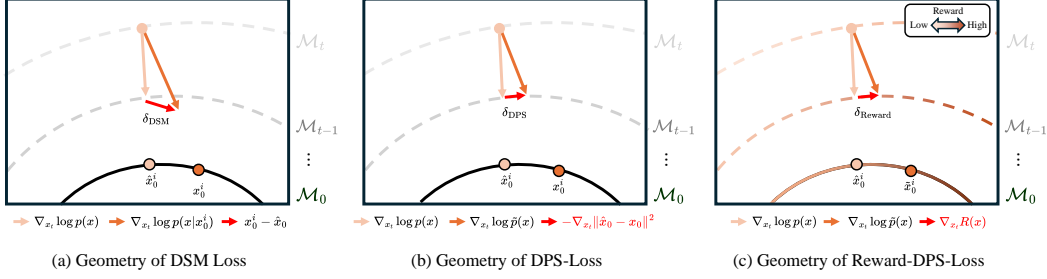


Figure 2: Conceptual illustration of the geometries of different losses. (a) Standard DSM loss shifts the score function toward the original image x_0^i (red arrow). (b) Our DPS-Loss isolates only the tangential component of this shift. (c) Similarly, Reward-DPS-Loss creates a tangential guidance component from the reward gradient.

noisy latent $x_t^i = \text{DDIMinv}(x_0^i, 0 \rightarrow t)$ from the train sample x_0^i . Combined with our DPS-Loss, this approach removes all sources of randomness from gradient computation, resulting in more robust influence estimates through improved gradient fidelity. Note that this approach is limited to measuring training gradients. When measuring utility gradients, our goal is to perform data attribution for concepts in any generation process, so we create x_t through DDIM sampling starting from $x_T \sim \mathcal{N}(0, I)$.

Gradient Normalization As observed by Xie et al. [51], varying loss magnitudes across timesteps can cause certain gradients to dominate attribution results. To address this, we normalize each timestep gradient g_t to unit norm, $\bar{g}_t = g_t / \|g_t\|_2$, ensuring that no single timestep exerts disproportionate influence on the final attribution score. Notably, this normalization makes our method invariant to hyperparameters such as β and w in the DPS loss, providing additional robustness.

We refer to the concept attribution method that incorporates all of the above techniques as *Concept-TRAK*, or C-TRAK for short, with the full algorithm summarized in Appendix E.

4 Geometric Interpretation of Concept-TRAK

To understand how our method captures concept-level attribution, we examine the geometric mechanism of *Concept-TRAK*.

The gradients of standard DSM loss and our proposed losses can be decomposed as:

$$\begin{aligned}\nabla_{\theta} \mathcal{L}_{\text{DSM}}(x_t; \theta) &= -2 \nabla_{\theta} \epsilon_{\theta}(x_t, t)^{\top} (\epsilon - \epsilon_{\theta}(x_t, t)) = -2 \mathbf{J}_{\text{DSM}}^{\top} \delta_{\text{DSM}}, \\ \nabla_{\theta} \mathcal{L}_{\text{DPS}}(x_t; \theta) &= -2 \nabla_{\theta} \epsilon_{\theta}(x_t, t)^{\top} \delta_{\text{DPS}} = -2 \mathbf{J}_{\text{DPS}}^{\top} \delta_{\text{DPS}}, \\ \nabla_{\theta} \mathcal{L}_{\text{Reward-DPS}}(x_t; \theta) &= -2 \nabla_{\theta} \epsilon_{\theta}(x_t, t)^{\top} \delta_{\text{Reward}} = -2 \mathbf{J}_{\text{Reward}}^{\top} \delta_{\text{Reward}},\end{aligned}$$

where $\delta_{\text{DSM}} = \epsilon - \epsilon_{\theta}(x_t, t)$, $\delta_{\text{DPS}} = \nabla_{x_t} \|x_0^i - \hat{x}_0^i\|^2$ and $\delta_{\text{Reward}} = -\nabla_{x_t} R(x_t)$ represent the guidance vectors arising from the training and reward objectives, respectively. $\mathbf{J} = \nabla_{\theta} \epsilon_{\theta}(x_t, t)$ denotes the Jacobian of the noise prediction network with respect to parameters θ .

Substituting these gradients into the influence function, with \mathcal{L}_{DPS} as the training loss and $\mathcal{L}_{\text{Reward-DPS}}$ as the utility function, we obtain:

$$\mathcal{I}(x_0^i, R) = \nabla_{\theta} \mathcal{L}_{\text{Reward-DPS}}^{\top} \mathbf{H}^{-1} \nabla_{\theta} \mathcal{L}_{\text{DPS}} = 4 \delta_{\text{Reward}}^{\top} \mathbf{J}_{\text{Reward}} \mathbf{H}^{-1} \mathbf{J}_{\text{DPS}}^{\top} \delta_{\text{DPS}},$$

where, $\mathbf{H} = \nabla_{\theta}^2 \mathcal{L}_{\text{train}}(D; \theta)$ is the Hessian of the training loss over the dataset D .

This reveals a key insight: *Concept-TRAK* quantifies the alignment between two guidance directions—one from a training sample and another from a reward-defined concept. But what does it mean for two guidance vectors to be similar, and why is this alignment a meaningful criterion for concept attribution?

To understand this, consider the latent space geometry illustrated in Figure 2. In diffusion models, the noise-perturbed data at each timestep t can be viewed as concentrated around a manifold (shell) \mathcal{M}_t

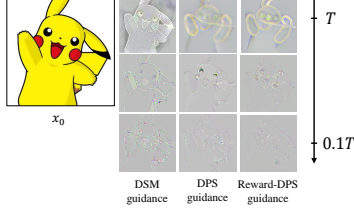


Figure 3: Visualization of guidance vectors at different timesteps.

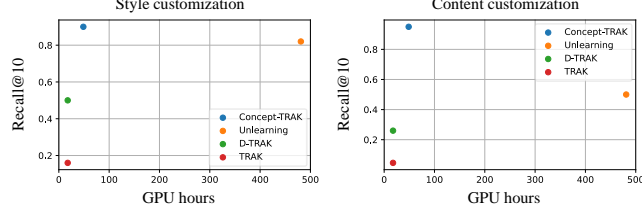


Figure 4: Quantitative performance comparisons on AbC benchmark.

with high probability [8, 7]. The score function $\nabla_{x_t} \log p_t(x)$ (light orange arrow) primarily works to project noisy samples back toward the clean data manifold \mathcal{M}_0 .

The key insight in our approach concerns how different loss functions interact with this manifold structure. As shown in Figure 2(a), the standard DSM loss involves the difference between unconditional and conditional score functions, i.e., δ_{DSM} , which combines both projection components (pointing toward the clean data manifold) and tangential components (operating within the current manifold level). In contrast, our DPS-Loss (Figure 2(b)) isolates primarily the tangential component through the gradient $\delta_{\text{DPS}} = -\nabla_{x_t} \|x_0^i - \hat{x}_0^i\|^2$ [8, 7]. Similarly, our Reward-DPS-Loss (Figure 2(c)) creates a tangential guidance component through the reward gradient $\delta_{\text{Reward}} = \nabla_{x_t} R(x_t)$.

This isolation of tangential components is crucial because they encode rich semantic information. Figure 3 demonstrates this empirically - both DPS and Reward-DPS guidance vectors maintain clean, consistent semantic structure across different timesteps of the diffusion process. This aligns with recent research showing that directions in the tangent space of diffusion models naturally correspond to interpretable concepts [30, 3, 49, 24].

For concept attribution, this geometric insight explains why our approach is effective: we’re measuring alignment between semantically meaningful tangential guidance directions rather than potentially noisy projections. When the guidance direction from a training sample x_0^i closely aligns with the guidance direction representing our target concept, it indicates that x_0^i substantially influenced the model’s ability to generate that specific concept.

5 Experiments

In this section, we evaluate *Concept-TRAK* across multiple concept attribution scenarios, comparing it against TRAK, D-TRAK, and an unlearning-based attribution method. Implementation details are provided in the appendix.

5.1 Attribution by Customization (AbC)

Following the setup in Wang et al. [47], we use the *Attribution by Customization* Benchmark (AbC), which evaluates attribution methods on models fine-tuned using one or a few exemplar images to learn new concepts with a special token $\langle V \rangle$. The AbC benchmark measures whether data attribution for images generated using this special token successfully retrieves the exemplars. This setup offers a rare source of ground truth: generated outputs are known to be directly influenced by the exemplars. While this setting lacks generality for large-scale training regimes, it remains the most reliable way to evaluate concept-level attribution in current text-to-image models.

Evaluation Protocol Given that the AbC Benchmark provides ground truth, we frame the problem as a retrieval task and report Recall@10—the proportion of times the exemplar images are successfully retrieved from a pool of 100K LAION images. We compare our method against TRAK [29], D-TRAK [52] and the unlearning-based attribution method (Unlearn) [48]. While the original benchmark involves not only learning exemplar using special tokens but also fine-tuning the model’s parameter on the exemplar dataset, real-world use cases more commonly involve investigating the concepts generated or utilized by a single pretrained model. To better reflect this, we adopt textual inversion [11] with a frozen base model (SD1.4v) [34], which only train with a special token $\langle V \rangle$, without parameter update. Further implementation details are provided in the Appendix D.



Figure 5: Qualitative results on the AbC benchmark. Correctly retrieved samples are highlighted with red boxes. Previous methods (Unlearn, D-TRAK) struggle with interference from style elements and retrieve unrelated images, while Ours successfully isolates target concepts $\langle V \rangle$.

Results Our method achieves significantly higher Recall@10 while maintaining computational efficiency comparable to TRAK-based method, as shown in Figure 4. As illustrated in Figure 5, prior methods often fail to isolate the concept of interest $\langle V \rangle$ due to interference from style or other visual elements in the generated image. In contrast, Concept-TRAK effectively isolates and attributes the target concept $\langle V \rangle$, demonstrating superior performance in concept-level attribution.

Ablation Study We conduct an ablation study using 48 samples from the AbC dataset to assess the impact of each design choice. Starting from the baseline TRAK with \mathcal{L}_{DSM} , adding concept-aware utility gradients (A), DPS-based training gradients (B), DDIM inversion (C), and gradient normalization (D) progressively improves performance, with our full method achieving 0.955 Recall@10.

Table 1: Ablation study.

Config	Recall@10 (\uparrow)
TRAK (Base: \mathcal{L}_{DSM})	0.04
+ (Config A: $\mathcal{L}_{\text{Reward-DPS}}$)	0.261
+ (Config B: \mathcal{L}_{DPS})	0.335
+ (Config C: DDIMInv)	0.564
+ (Config D: Normalize)	0.955

5.2 Applications of Concept-Level Attribution

Our concept-level attribution method provides valuable insights across multiple domains, as shown in Figure 6. For **copyright protection**, we trace training samples that influenced IP-protected concepts like Mario and Mickey Mouse, addressing provenance concerns. In the realm of **safety**, our method identifies training samples contributing to sensitive concepts, enabling targeted data curation for responsible AI development. For **model debugging**, Concept-TRAK pinpoints sources of both desirable features and problematic outputs, enhancing our understanding of prompt engineering. Finally, for **concept learning**, our approach reveals how models acquire complex relational concepts like “hug” and “shake hands.”. These applications demonstrate how concept-level attribution provides practical tools for addressing key challenges in generative AI development and governance.

6 Related Work

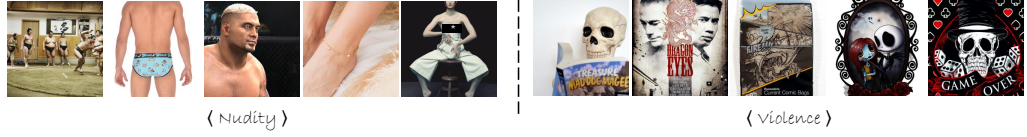
Data Attribution Established data attribution methods include influence functions [32], which approximate leave-one-out retraining via gradients. TRAK and LoGra [29, 6] improve scalability through random projections. Game-theoretic approaches like Data Shapley [21, 14], based on Shapley values [37], were initially limited by retraining costs, but recent work [45, 46] improves efficiency by removing this requirement. Unlearning-based methods [48] offer alternative trade-offs between efficiency and theoretical rigor.

Data Attribution for Diffusion Models Early diffusion attribution methods adapted influence functions [32, 29], but were biased by timestep-dependent gradient norms. Xie et al. [51] addressed this via a re-normalized formulation. Zheng et al. [52] extended TRAK to diffusion models, exploiting its scalability. Lin et al. [23] later proposed the Diffusion Attribution Score, which quantifies per-sample influence by directly comparing predicted distributions, yielding more precise attributions than loss-based approaches.

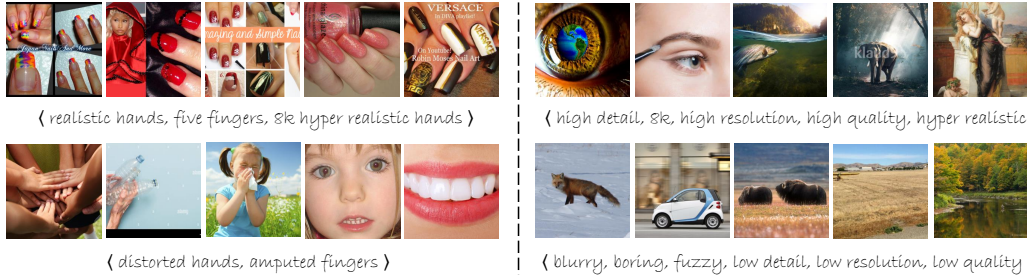
(a) Identify IP-protected contents



(b) Detect Unsafe contents



(c) Model debugging



(d) Understand concept learning

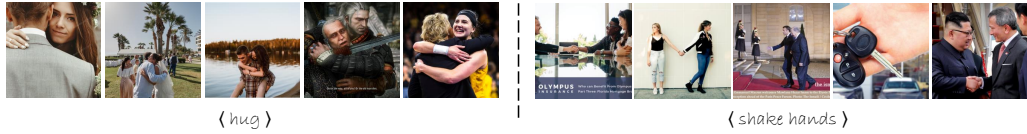


Figure 6: Applications of concept-level attribution across diverse tasks. (a) Identifying training sources of IP-protected characters. (b) Detecting origins of sensitive content for safety governance. (c) Tracing sources of desirable and problematic features for model debugging. (d) Revealing how models acquire relational concept understanding.

7 Conclusion

We propose *Concept-TRAK*, a method for concept-level attribution that extends influence functions to trace how training data affects specific semantic components of model outputs. It introduces (1) a reformulated diffusion loss via diffusion posterior sampling for robust, sample-specific gradients, and (2) a concept-aware reward to enhance semantic alignment. Concept-TRAK outperforms existing methods on the AbC benchmark and demonstrates effective in diverse tasks like unsafe content detection, prompt analysis, and compositional concept learning—offering actionable insights for responsible generative AI development.

References

- [1] Emmanuel Bengio, Moksh Jain, Maksym Korablyov, Doina Precup, and Yoshua Bengio. Flow network based generative models for non-iterative diverse candidate generation. *Advances in Neural Information Processing Systems*, 34:27381–27394, 2021.
- [2] Yoshua Bengio, Salem Lahlou, Tristan Deleu, Edward J Hu, Mo Tiwari, and Emmanuel Bengio. Gflownet foundations. *Journal of Machine Learning Research*, 24(210):1–55, 2023.
- [3] Manuel Brack, Felix Friedrich, Dominik Hintersdorf, Lukas Struppek, Patrick Schramowski, and Kristian Kersting. Sega: Instructing text-to-image models using semantic guidance. *Advances in Neural Information Processing Systems*, 36:25365–25389, 2023.
- [4] Blake Brittain. Getty images lawsuit says stability ai misused photos to train ai. *Reuters*, February 2023. URL <https://www.reuters.com/legal/getty-images-lawsuit-says-stability-ai-misused-photos-train-ai-2023-02-06/>.
- [5] Nicolas Carlini, Jamie Hayes, Milad Nasr, Matthew Jagielski, Vikash Sehwal, Florian Tramer, Borja Balle, Daphne Ippolito, and Eric Wallace. Extracting training data from diffusion models. In *32nd USENIX Security Symposium (USENIX Security 23)*, pages 5253–5270, 2023.
- [6] Sang Keun Choe, Hwijee Ahn, Juhan Bae, Kewen Zhao, Minsoo Kang, Youngseog Chung, Adithya Pratapa, Willie Neiswanger, Emma Strubell, Teruko Mitamura, et al. What is your data worth to gpt? llm-scale data valuation with influence functions. *arXiv preprint arXiv:2405.13954*, 2024.
- [7] Hyungjin Chung, Jeongsol Kim, Michael T Mccann, Marc L Klasky, and Jong Chul Ye. Diffusion posterior sampling for general noisy inverse problems. *arXiv preprint arXiv:2209.14687*, 2022.
- [8] Hyungjin Chung, Byeongsu Sim, Dohoon Ryu, and Jong Chul Ye. Improving diffusion models for inverse problems using manifold constraints. *Advances in Neural Information Processing Systems*, 35:25683–25696, 2022.
- [9] Junwei Deng, Shiyuan Zhang, and Jiaqi Ma. Computational copyright: Towards a royalty model for music generative ai. *arXiv preprint arXiv:2312.06646*, 2023.
- [10] Patrick Esser, Sumith Kulal, Andreas Blattmann, Rahim Entezari, Jonas Müller, Harry Saini, Yam Levi, Dominik Lorenz, Axel Sauer, Frederic Boesel, et al. Scaling rectified flow transformers for high-resolution image synthesis. In *Forty-first International Conference on Machine Learning*, 2024.
- [11] Rinon Gal, Yuval Alaluf, Yuval Atzmon, Or Patashnik, Amit H Bermano, Gal Chechik, and Daniel Cohen-Or. An image is worth one word: Personalizing text-to-image generation using textual inversion. *arXiv preprint arXiv:2208.01618*, 2022.
- [12] Rohit Gandikota, Joanna Materzyńska, Tingrui Zhou, Antonio Torralba, and David Bau. Concept sliders: Lora adaptors for precise control in diffusion models. In *European Conference on Computer Vision*, pages 172–188. Springer, 2024.
- [13] GenLaw2024. 2nd workshop on generative ai and law (genlaw ’24). <https://www.genlaw.org/2024-icml>, July 2024. Held at the International Conference on Machine Learning (ICML) 2024, Vienna, Austria.
- [14] Amirata Ghorbani and James Zou. Data shapley: Equitable valuation of data for machine learning. In Kamalika Chaudhuri and Ruslan Salakhutdinov, editors, *Proceedings of the 36th International Conference on Machine Learning*, volume 97 of *Proceedings of Machine Learning Research*, pages 2242–2251. PMLR, 09–15 Jun 2019. URL <https://proceedings.mlr.press/v97/ghorbani19c.html>.
- [15] Roger Grosse, Juhan Bae, Cem Anil, Nelson Elhage, Alex Tamkin, Amirhossein Tajdini, Benoît Steiner, Dustin Li, Esin Durmus, Ethan Perez, et al. Studying large language model generalization with influence functions. *arXiv preprint arXiv:2308.03296*, 2023.

- [16] Jonathan Ho and Tim Salimans. Classifier-free diffusion guidance. *arXiv preprint arXiv:2207.12598*, 2022.
- [17] Jonathan Ho, Ajay Jain, and Pieter Abbeel. Denoising diffusion probabilistic models. *Advances in Neural Information Processing Systems*, 33:6840–6851, 2020.
- [18] Chris C Holmes and Stephen G Walker. Assigning a value to a power likelihood in a general bayesian model. *Biometrika*, 104(2):497–503, 2017.
- [19] Chin-Wei Huang, Jae Hyun Lim, and Aaron Courville. A variational perspective on diffusion-based generative models and score matching. In A. Beygelzimer, Y. Dauphin, P. Liang, and J. Wortman Vaughan, editors, *Advances in Neural Information Processing Systems*, 2021. URL <https://openreview.net/forum?id=bXehDYUjjXi>.
- [20] Ruoxi Jia, David Dao, Boxin Wang, Frances Ann Hubis, Nezihe Merve Gurel, Bo Li, Ce Zhang, Costas J Spanos, and Dawn Song. Efficient task-specific data valuation for nearest neighbor algorithms. *arXiv preprint arXiv:1908.08619*, 2019.
- [21] Ruoxi Jia, David Dao, Boxin Wang, Frances Ann Hubis, Nick Hynes, Nezihe Merve Gürel, Bo Li, Ce Zhang, Dawn Song, and Costas J. Spanos. Towards efficient data valuation based on the shapley value. In Kamalika Chaudhuri and Masashi Sugiyama, editors, *Proceedings of the Twenty-Second International Conference on Artificial Intelligence and Statistics*, volume 89 of *Proceedings of Machine Learning Research*, pages 1167–1176. PMLR, 16–18 Apr 2019. URL <https://proceedings.mlr.press/v89/jia19a.html>.
- [22] Pang Wei Koh and Percy Liang. Understanding black-box predictions via influence functions. In *International conference on machine learning*, pages 1885–1894. PMLR, 2017.
- [23] Jinxu Lin, Linwei Tao, Minjing Dong, and Chang Xu. Diffusion attribution score: Evaluating training data influence in diffusion model. In *The Thirteenth International Conference on Learning Representations*, 2025. URL <https://openreview.net/forum?id=kuutidLf6R>.
- [24] Nan Liu, Shuang Li, Yilun Du, Antonio Torralba, and Joshua B Tenenbaum. Compositional visual generation with composable diffusion models. In *European Conference on Computer Vision*, pages 423–439. Springer, 2022.
- [25] Zhen Liu, Tim Z Xiao, Weiyang Liu, Yoshua Bengio, and Dinghuai Zhang. Efficient diversity-preserving diffusion alignment via gradient-informed gflownets. *arXiv preprint arXiv:2412.07775*, 2024.
- [26] Taywon Min, Haeone Lee, Hanho Ryu, Yongchan Kwon, and Kimin Lee. Understanding impact of human feedback via influence functions. *arXiv preprint arXiv:2501.05790*, 2025.
- [27] Bruno Mlodozieniec, Runa Eschenhagen, Juhan Bae, Alexander Immer, David Krueger, and Richard Turner. Influence functions for scalable data attribution in diffusion models. *arXiv preprint arXiv:2410.13850*, 2024.
- [28] Alex Nichol, Prafulla Dhariwal, Aditya Ramesh, Pranav Shyam, Pamela Mishkin, Bob McGrew, Ilya Sutskever, and Mark Chen. Glide: Towards photorealistic image generation and editing with text-guided diffusion models. *arXiv preprint arXiv:2112.10741*, 2021.
- [29] Sung Min Park, Kristian Georgiev, Andrew Ilyas, Guillaume Leclerc, and Aleksander Mądry. Trak: attributing model behavior at scale. In *Proceedings of the 40th International Conference on Machine Learning*, pages 27074–27113, 2023.
- [30] Yong-Hyun Park, Mingi Kwon, Jaewoong Choi, Junghyo Jo, and Youngjung Uh. Understanding the latent space of diffusion models through the lens of riemannian geometry. *Advances in Neural Information Processing Systems*, 36:24129–24142, 2023.
- [31] Dustin Podell, Zion English, Kyle Lacey, Andreas Blattmann, Tim Dockhorn, Jonas Müller, Joe Penna, and Robin Rombach. Sdxl: Improving latent diffusion models for high-resolution image synthesis. *arXiv preprint arXiv:2307.01952*, 2023.

- [32] Garima Pruthi, Frederick Liu, Satyen Kale, and Mukund Sundararajan. Estimating training data influence by tracing gradient descent. *Advances in Neural Information Processing Systems*, 33: 19920–19930, 2020.
- [33] Rafael Rafailov, Archit Sharma, Eric Mitchell, Christopher D Manning, Stefano Ermon, and Chelsea Finn. Direct preference optimization: Your language model is secretly a reward model. *Advances in Neural Information Processing Systems*, 36:53728–53741, 2023.
- [34] Robin Rombach, Andreas Blattmann, Dominik Lorenz, Patrick Esser, and Björn Ommer. High-resolution image synthesis with latent diffusion models. In *Proceedings of the IEEE/CVF conference on computer vision and pattern recognition*, pages 10684–10695, 2022.
- [35] Laura Ruis, Maximilian Mozes, Juhan Bae, Siddhartha Rao Kamalakara, Dwarak Talupuru, Acyr Locatelli, Robert Kirk, Tim Rocktäschel, Edward Grefenstette, and Max Bartolo. Procedural knowledge in pretraining drives reasoning in large language models. *arXiv preprint arXiv:2411.12580*, 2024.
- [36] Christoph Schuhmann, Romain Beaumont, Richard Vencu, Cade Gordon, Ross Wightman, Mehdi Cherti, Theo Coombes, Aarush Katta, Clayton Mullis, Mitchell Wortsman, et al. Laion-5b: An open large-scale dataset for training next generation image-text models. *Advances in neural information processing systems*, 35:25278–25294, 2022.
- [37] Lloyd S Shapley et al. A value for n-person games. 1953.
- [38] Jascha Sohl-Dickstein, Eric Weiss, Niru Maheswaranathan, and Surya Ganguli. Deep unsupervised learning using nonequilibrium thermodynamics. In *International Conference on Machine Learning*, pages 2256–2265. PMLR, 2015.
- [39] Gowthami Somepalli, Vasu Singla, Micah Goldblum, Jonas Geiping, and Tom Goldstein. Diffusion art or digital forgery? investigating data replication in diffusion models. In *Proceedings of the IEEE/CVF conference on computer vision and pattern recognition*, pages 6048–6058, 2023.
- [40] Gowthami Somepalli, Vasu Singla, Micah Goldblum, Jonas Geiping, and Tom Goldstein. Understanding and mitigating copying in diffusion models. *Advances in Neural Information Processing Systems*, 36:47783–47803, 2023.
- [41] Jiaming Song, Chenlin Meng, and Stefano Ermon. Denoising diffusion implicit models. In *International Conference on Learning Representations*, 2021.
- [42] Yang Song, Jascha Sohl-Dickstein, Diederik P Kingma, Abhishek Kumar, Stefano Ermon, and Ben Poole. Score-based generative modeling through stochastic differential equations. In *International Conference on Learning Representations*, 2021.
- [43] Pascal Vincent. A connection between score matching and denoising autoencoders. *Neural computation*, 23(7):1661–1674, 2011.
- [44] Bram Wallace, Meihua Dang, Rafael Rafailov, Linqi Zhou, Aaron Lou, Senthil Purushwalkam, Stefano Ermon, Caiming Xiong, Shafiq Joty, and Nikhil Naik. Diffusion model alignment using direct preference optimization. In *Proceedings of the IEEE/CVF Conference on Computer Vision and Pattern Recognition*, pages 8228–8238, 2024.
- [45] Jiachen T Wang, Yuqing Zhu, Yu-Xiang Wang, Ruoxi Jia, and Prateek Mittal. Threshold knn-shapley: A linear-time and privacy-friendly approach to data valuation. *arXiv preprint arXiv:2308.15709*, 2023.
- [46] Jiachen T Wang, Prateek Mittal, Dawn Song, and Ruoxi Jia. Data shapley in one training run. *arXiv preprint arXiv:2406.11011*, 2024.
- [47] Sheng-Yu Wang, Alexei A Efros, Jun-Yan Zhu, and Richard Zhang. Evaluating data attribution for text-to-image models. In *Proceedings of the IEEE/CVF International Conference on Computer Vision*, pages 7192–7203, 2023.
- [48] Sheng-Yu Wang, Aaron Hertzmann, Alexei Efros, Jun-Yan Zhu, and Richard Zhang. Data attribution for text-to-image models by unlearning synthesized images. *Advances in Neural Information Processing Systems*, 37:4235–4266, 2024.

- [49] Zihao Wang, Lin Gui, Jeffrey Negrea, and Victor Veitch. Concept algebra for (score-based) text-controlled generative models. *Advances in Neural Information Processing Systems*, 36: 35331–35349, 2023.
- [50] Yuxin Wen, Yuchen Liu, Chen Chen, and Lingjuan Lyu. Detecting, explaining, and mitigating memorization in diffusion models. In *The Twelfth International Conference on Learning Representations*, 2024. URL <https://openreview.net/forum?id=84n3UwkH7b>.
- [51] Tong Xie, Haoyu Li, Andrew Bai, and Cho-Jui Hsieh. Data attribution for diffusion models: Timestep-induced bias in influence estimation. *Transactions on Machine Learning Research*, 2024.
- [52] Xiaosen Zheng, Tianyu Pang, Chao Du, Jing Jiang, and Min Lin. Intriguing properties of data attribution on diffusion models. In *The Twelfth International Conference on Learning Representations*, 2024.

A Discussions

Limitations and Future Work Our research advances beyond traditional data attribution by identifying training samples that specifically contribute to particular concepts. While we demonstrated *Concept-TRAK*’s superior performance in concept-level attribution compared to existing data attribution methods on the AbC benchmark, our approach exhibits certain limitations. As illustrated in Figure 6(a) with the Simpsons example, our method occasionally retrieves stylistically similar but conceptually distinct images (e.g., other cartoon characters rather than Simpsons-specific content).

We hypothesize that this limitation stems from the fundamental challenge of gradient estimation in diffusion models. While our DPS-loss successfully eliminates Monte Carlo sampling from the standard DSM loss and provides more robust gradient estimates, perfect gradient estimation would theoretically require the true DSM loss computed with infinite Monte Carlo samples over both the noise term ϵ and noisy latents x_t . Our deterministic approximation, though significantly improved, cannot fully capture this infinite sampling complexity. Consequently, some attribution errors persist.

For concept-level attribution to serve as a reliable tool for addressing copyright concerns and enabling model debugging, further development is required in two key areas: (1) establishing more sophisticated benchmarks that measure concept-level attribution performance across diverse concept types and contexts, and (2) enhancing the precision and theoretical guarantees of concept-level attribution methods. This work represents an initial investigation that introduces the concept-level attribution problem and proposes *Concept-TRAK* as a foundational framework, and we anticipate that these contributions will catalyze further research into more robust concept-level attribution methods suitable for increasingly sophisticated generative models.

Impact Statements While our work provides tools for analyzing training data and understanding diffusion models for image generation without direct safety concerns, there exists potential for misuse by model developers who might exploit our tools to learn unsafe or problematic concepts. We emphasize that our method is intended for responsible model development and governance, including the identification and mitigation of harmful content in training datasets.

B Theoretical Details

In this section, we provide the derivation for the DPS-Loss introduced in Section 3.1. Our objective is to model how upweighting an individual training sample x_0^i influences the model. We formulate this using a generalized Bayesian update with power likelihood:

$$p(\theta \mid D) \propto p(D \mid \theta)^w p(\theta),$$

where $D = \{x_0^i\}$, and we treat the model output x as analogous to parameters θ , resulting in:

$$p(x \mid x_0^i) \propto p(x_0^i \mid x)^w p(x).$$

The key quantity required for DPS-Loss is the posterior $p(x_0^i \mid x_t)$, where x_t denotes the noisy latent at diffusion timestep t . We derive it as:

$$\begin{aligned} p(x_0^i \mid x_t) &= \int p(x_0^i, x_0 \mid x_t) dx_0 \\ &= \int p(x_0^i \mid x_0, x_t) p(x_0 \mid x_t) dx_0. \end{aligned}$$

To approximate this integral, we make two assumptions:

- **Delta approximation:** We approximate $p(x_0 \mid x_t)$ with a Dirac delta function centered at the denoised estimate $\hat{x}_0 = \mathbb{E}[x_0 \mid x_t]$: $p(x_0 \mid x_t) \approx \delta(x_0 - \hat{x}_0)$
- **Gaussian assumption:** We assume the data distribution is locally approximated by a Gaussian distribution, such that:

$$p(x_0^i \mid x_0) \propto \exp(-\|x_0^i - x_0\|_2^2).$$

Applying these approximations yields:

$$p(x_0^i \mid x_t) \approx p(x_0^i \mid \hat{x}_0) \propto \exp(-\|x_0^i - \hat{x}_0\|_2^2).$$

This approximation allows us to compute an analytic estimate of the influence function gradient without requiring model retraining for each upweighted data point.

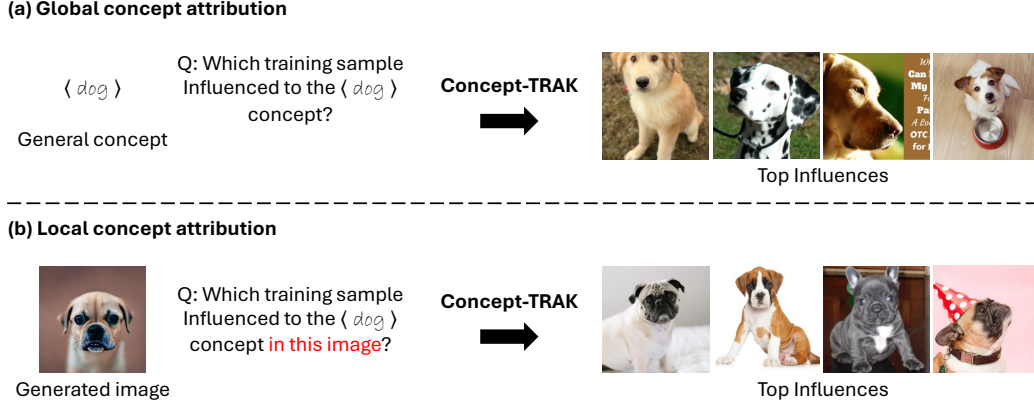


Figure 7: (a) Global concept attribution identifies training samples that influenced the learning of general concepts across all generations. (b) Local concept attribution identifies training samples that influenced the learning of specific concept manifestations appearing in a particular generated image. For example, when applying local concept attribution to the “dog” concept in a generated image of a bulldog-like dog, we can observe that it retrieves images similar to bulldogs, demonstrating more targeted attribution.

C Other Types of Reward

In this section, we show how to apply *Concept-TRAK* beyond textual concepts. We cover three scenarios: local concept attribution, explicit differentiable reward models, and implicit reward models defined by preference datasets.

C.1 Local Concept Attribution

Our main experiments focused on attributing general concepts c for every sampling trajectory, rather than specific concepts c that are used in a particular generation of synthesized image x_{test} . This approach performs concept-level attribution across all sampling paths, which we can call *global concept attribution*.

In contrast, we may want to measure concept attribution for a concept c_{test} appearing in a specific generated image. We refer to this case as *local concept attribution*. To illustrate the difference: global concept attribution measures how a general concept (e.g., “dog”) was learned, identifying training samples that contributed to the model’s overall understanding of dogs (Figure 7(a)). This general concept knowledge influences the sampling process across many different generated images. Local concept attribution, however, measures which specific training samples influenced the generation of a particular dog image when the model generates it—focusing on the specific characteristics of that individual generated instance rather than the general concept. As shown in Figure 7(b), when we apply local attribution to a bulldog-like generated image, it specifically retrieves bulldog training samples rather than diverse dog breeds. In this subsection, we introduce how to apply our method to this scenario.

The key insight for local concept attribution is that we should use $p(c_{\text{test}}|x)$ as the reward instead of $p(c|x)$. One approach is to discover c_{test} through textual inversion [11], enabling attribution for the specific concept as it appears in the generated image rather than the general concept c . Preliminary results for this approach are provided in Appendix F.

C.2 External Differentiable Reward Models

An explicit, differentiable reward model $R(\hat{x}_i^0)$ may be used to quantify the presence of a concept in the generated image \hat{x}_i^0 (e.g., detecting whether a person is wearing glasses). In this case, similar to our earlier approach, for rewards defined on clean images, we approximate $\nabla_{x_t} R(x) \approx \nabla_{x_t} R(\hat{x}_i^0)$.

This yields our Reward-DPS loss:

$$\mathcal{L}_{\text{Reward-DPS}}(x_t; \theta) = \left\| \text{sg} \left[\epsilon_\theta(x_t, t) - \frac{1}{\beta} \cdot \nabla_{x_t} R(\hat{x}_i^0) \right] - \epsilon_\theta(x_t, t) \right\|_2^2.$$

It is worth noting that this loss produces gradients equivalent to those from ∇ -DB [25] at initialization. However, the derivation and formulation differ significantly: our approach is based on DPS principles, while Liu et al. [25] is derived from GFlowNet foundations [1, 2], resulting in fundamentally different loss functions despite the similar gradient form at initialization.

C.3 Preference Datasets

For preference datasets, one approach would be to first train an explicit reward model and then use the trained reward model to compute utility gradients as described earlier. However, inspired by Direct Preference Optimization (DPO) [33], we can also work with an implicit reward model directly. Here we present a method for measuring utility gradients through an implicit reward formulation.

Given preference pairs (x^+, x^-) , we can define a Bradley-Terry reward model: $p(x^+ \succ x^-) = \sigma(r(x^+) - r(x^-))$, where $x^+ \succ x^-$ means x^+ is preferred over x^- , σ is the logistic function, and $r(\cdot)$ is the reward model. Following the DPO framework [33], the reward model implied by preference data has the relationship:

$$r(x) = \beta \log \frac{p_\theta(x)}{p_\phi(x)} + \beta Z. \quad (2)$$

Here, p_θ represents the probability under a model fine-tuned with the reward, while p_ϕ is the probability under the original pretrained model, and β corresponds to the kl divergence regularization term between p_θ and p_ϕ used in reward maximization.

DPO learns directly train p_θ through maximizing $p(x^+ \succ x^-)$ where they replace the reward using Eq. equation 2. The corresponding loss function is:

$$\mathcal{L}_{\text{DPO}} = -\mathbb{E}_{(x^+, x^-)} \left[\log \sigma \left(\beta \log \frac{p_\theta(x^+)}{p_\phi(x^+)} - \beta \log \frac{p_\theta(x^-)}{p_\phi(x^-)} \right) \right].$$

In the context of diffusion models, we need to translate this into terms of the denoising score matching loss. For diffusion models, the log probability can be expressed through the DSM loss as $\log p(x) \approx -\mathbb{E}_{t, \epsilon} [\|\epsilon - \epsilon_\theta(x_t, t)\|^2]$. Therefore, the diffusion-specific DPO loss becomes [44]:

$$\mathcal{L}_{\text{DiffusionDPO}} = -\mathbb{E}_{(x^+, x^-) \sim \mathcal{D}} \log \sigma \left[-\beta (\|\epsilon - \epsilon_\theta(x_t^-, t)\|^2 - \|\epsilon - \epsilon_\theta(x_t^+, t)\|^2) \right].$$

This formulation encourages the model to assign higher probability to preferred samples x^+ and lower probability to less preferred samples x^- .

For our purposes, we need $R(x^+, x^-) = r(x^+) - r(x^-)$ and its gradient with respect to x_t :

$$\nabla_{x_t} R(x^+, x^-) = \nabla_{x_t} \log \frac{p_\theta(x^+)}{p_\phi(x^+)} - \nabla_{x_t} \log \frac{p_\theta(x^-)}{p_\phi(x^-)}.$$

However, we face a challenge similar to our DPS-Loss: we don't have access to the fine-tuned model p_θ that would result from training on the preference dataset. To address this, we apply the same approximation technique used in our DPS-Loss, treating the preference pairs as guidance signals that modify the score function through our Gaussian approximation framework.

Using our established approximation p_θ based on generalized Bayesian framework, i.e., $p_\theta(x) \propto p(x) \cdot p(x|x^+)^w \cdot (1/p(x|x^-))^w$, and Gaussian assumption, i.e., $p(x|x^i) \propto \exp(-\|x - x^i\|^2)$ (Section 3.1). We can approximate p_θ as:

$$\begin{aligned} \nabla_{x_t} \log p_\theta(x^+) &= \nabla_{x_t} \log p_\phi(x^+) + w \nabla_{x_t} \log p(x^+|x^+) - w \nabla_{x_t} \log p(x^+|x^-) \\ &\approx \nabla_{x_t} \log p_\phi(x^+) - w \nabla_{x_t} \|\hat{x}_0^+ - x^+\|_2^2 + w \nabla_{x_t} \|\hat{x}_0^+ - x^-\|_2^2. \end{aligned}$$

where \hat{x}_0^+ denotes the predicted clean image corresponding to the noisy sample derived from x^+ .

After substituting all terms into $\nabla_{x_t} R(x^+, x^-)$ and applying our Gaussian approximations, we obtain:

$$\begin{aligned}\nabla_{x_t} R(x^+, x^-) &= \nabla_{x_t} \log p(x_t^+ | x^+) + \nabla_{x_t} \log p(x_t^- | x^+) \\ &\quad - \nabla_{x_t} \log p(x_t^+ | x^-) - \nabla_{x_t} \log p(x_t^- | x^-) \\ &= -(\nabla_{x_t} \|\hat{x}_0^+ - x^+\|_2^2 + \nabla_{x_t} \|\hat{x}_0^- - x^+\|_2^2) \\ &\quad + (\nabla_{x_t} \|\hat{x}_0^+ - x^-\|_2^2 + \nabla_{x_t} \|\hat{x}_0^- - x^-\|_2^2).\end{aligned}$$

Here, we set the upweight scale w as 1, since the normalization of the gradient will make the gradient invariant to the upweight scale (Section 3.3). This utility gradient can then be incorporated into our Reward-DPS-Loss, enabling concept attribution with preference data without explicitly training a reward model.

D Implementation Details

Computational Resources All experiments were conducted on NVIDIA H100 GPUs with 80GB memory. To reduce computational costs, all experiments were performed using fp16 precision. For AbC benchmark, the computational requirements for different components are as follows:

- **Textual inversion training:** Approximately 30 minutes per customization dataset on a single H100 GPU, totaling 10 GPU hours for all datasets.
- **Unlearning:** Computing the loss for the entire training dataset requires 1.2 GPU hours. For the complete AbC benchmark evaluation, this totals 480 GPU hours.
- **TRAK, D-TRAK:** Computing training gradients requires around 17 GPU hours. Computing utility gradients takes less than 30 seconds, which is negligible. Total: 17.6 GPU hours.
- **Concept-TRAK:** Our method requires additional time due to guidance computation in the DPS-Loss. Computing training gradients requires around 23 GPU hours, and computing utility gradients for each concept take approximately 5 minutes. Total experimental time: 52.4 GPU hours.

D.1 AbC Benchmark

This subsection presents the detailed experimental setup for our evaluation of the AbC benchmark.

Benchmark Construction To address more realistic data attribution scenarios, we modify the original AbC benchmark setup. Rather than fine-tuning model parameters on customization data, we freeze the base model parameters and train only special tokens through textual inversion [11]. Following Wang et al. [47], we create 20 special tokens corresponding to 20 customization concepts. For each special token, we generate 20 images, resulting in 400 total generated images for data attribution evaluation.

We perform textual inversion using the default hyperparameters provided by the diffusers library: AdamW optimizer with learning rate 5.0×10^{-4} , batch size 4, and training epochs 3000.

Baseline Methods Both TRAK and D-TRAK need to specify a regularization hyperparameter λ . To be more specific, in TRAK [29], we approximate the inverted projected Hessian as $\mathbf{H}_P^{-1} \approx (\mathbf{F}_P + \lambda I)^{-1}$, where $\mathbf{F}_P = \frac{1}{N} \sum_k G^\top G$ and $G_{ij} = \nabla_{\theta_j} L(x_i; \theta)$. The regularization λ is applied to make sure to $\mathbf{H}_P \approx \mathbf{F}_P + \lambda I$ is invertible in practice. On the other hand, this regularization makes TRAK-based data attribution effectively ignore components with small eigenvalues, significantly impacting attribution performance [6].

Previous work recommends $\lambda^* = 0.1 \times \text{mean}(\text{eigenvalues}(\mathbf{F}_P))$ [15]. For a fair comparison, we perform a hyperparameter sweep for TRAK and D-TRAK across $\lambda \in [\lambda^* \times 10^{-4}, \lambda^* \times 10^4]$ and report the best performance achieved.

Concept-TRAK Configuration Our method focuses on measuring contributions to specific concepts c . We use the synthetic image generation prompt as c^+ (e.g., “a tattoo of $\langle V \rangle$ snake”) and

remove only the special token to create c^- (e.g., “a tattoo of snake”). We used c^+ as the base prompt c . We set the regularization parameter to the recommended value $\lambda^* = 0.1 \times \text{mean}(\text{eigenvalues}(\mathbf{F}_P))$ [15] and use 1024 x_t from random trajectories sampled from DDIM sampler for gradient computation.

D.2 Qualitative Results

For the qualitative case studies presented in Section 5.2, we maintain consistent experimental settings with the AbC benchmark evaluation. The regularization parameter is set to $\lambda = 0.1 \times \text{mean}(\text{eigenvalues}(\mathbf{F}_P))$ across all methods. The concept prompts c^+ , c^- , and c are constructed following the contrastive approach described in Section 3.2, where positive and negative prompts isolate specific semantic concepts of interest.

Below are the prompts used for each concept-level attribution task:

- **IP-protected content:**
 - Mario:
 - $c^+ = \text{"character, Mario"}$
 - $c^- = \text{"character"}$
 - $c = \text{"character"}$
 - Mickey Mouse:
 - $c^+ = \text{"character, Mickey Mouse"}$
 - $c^- = \text{"character"}$
 - $c = \text{"character"}$
 - Simpsons:
 - $c^+ = \text{"character, Simpsons"}$
 - $c^- = \text{"character"}$
 - $c = \text{"character"}$
- **Unsafe content:**
 - Nudity:
 - $c^+ = \text{"person, nude, naked"}$
 - $c^- = \text{"person"}$
 - $c = \text{"person"}$
 - Violence:
 - $c^+ = \text{"zombie, bloody, violence, gore, horror, grotesque, skull, fear, death, creature"}$
 - $c^- = \text{" "}$
 - $c = \text{" "}$
- **Model debugging:**
 - Distorted hands:
 - $c^+ = \text{"hands, distorted hands, amputated fingers"}$
 - $c^- = \text{"realistic hands, five fingers, 8k hyper realistic hands"}$
 - $c = \text{"hands"}$
 - High quality images:
 - $c^+ = \text{"high detail, 8k, intricate, detailed, high resolution, high res, high quality, hyper realistic"}$
 - $c^- = \text{"blurry, boring, fuzzy, low detail, low resolution, low res, low quality"}$
 - $c = \text{" "}$
- **Concept learning:**
 - Hug:
 - $c^+ = \text{"people hug each other"}$
 - $c^- = \text{"people"}$
 - $c = \text{"people"}$
 - Shake hands:

$c^+ = \text{"people shake their hands"}$
 $c^- = \text{"people"}$
 $c = \text{"people"}$

Note on Model debugging For the model debugging study, we perform bidirectional attribution by swapping c^+ and c^- to identify both positive and negative influences. This allows us to trace training samples that contribute to both problematic and desirable generation.

E Algorithm

In this section, we provide detailed algorithms for computing training gradients using DPS-loss (Algorithm 1) and utility gradients using Reward-DPS-loss (Algorithm 2) used in *Concept-TRAK*. The key computational steps highlighted in red show the guidance terms that distinguish our approach from standard methods.

Algorithm 1 DPS-Loss

Require: $x_0^i, N, \{\bar{\alpha}_t\}_{t=0}^T$

- 1: **for** $n = 1$ **to** N **do**
- 2: $x_t^i \leftarrow \text{DDIMinv}(x_0^i, 0 \rightarrow \frac{nT}{N}), t \leftarrow \frac{nT}{N}$
- 3: $\hat{x}_0^i \leftarrow \frac{1}{\sqrt{\bar{\alpha}_t}} (x_t^i - \sqrt{1 - \bar{\alpha}_t} \epsilon_\theta(x_t^i))$
- 4: $\delta_{\text{DPS}} \leftarrow -\nabla_{x_t} \|\hat{x}_0^i - x_0^i\|_2^2$
- 5: $\tilde{\epsilon}_\theta(x_t^i) \leftarrow \text{sg}[\epsilon_\theta(x_t^i) - \delta_{\text{DPS}}]$
- 6: $\mathcal{L}_{\text{DPS}} \leftarrow \|\tilde{\epsilon}_\theta(x_t^i) - \epsilon_\theta(x_t^i)\|_2^2$
- 7: $g_n \leftarrow \nabla_\theta \mathcal{L}_{\text{DPS}}$
- 8: **end for**
- 9: $g \leftarrow \frac{1}{N} \sum_{n=1}^N g_n / \|g_n\|_2$
- 10: **return** g

Algorithm 2 Reward-DPS-Loss

Require: $N, \{\bar{\alpha}_t\}_{t=0}^T, \{\eta_t\}_{t=0}^T$

- 1: **for** $n = 1$ **to** N **do**
- 2: $x_T \sim \mathcal{N}(0, I), t \sim \text{Uniform}(0, T)$
- 3: $x_t \leftarrow \text{DDIM}(x_T, T \rightarrow t)$
- 4: $\hat{x}_0 \leftarrow \frac{1}{\sqrt{\bar{\alpha}_t}} (x_t - \sqrt{1 - \bar{\alpha}_t} \epsilon_\theta(x_t, t))$
- 5: $\delta_{\text{Reward-DPS}} \leftarrow \nabla_{x_t} R(x_t)$
- 6: $\tilde{\epsilon}_\theta(x_t, t) \leftarrow \text{sg}[\epsilon_\theta(x_t, t) - \delta_{\text{Reward-DPS}}]$
- 7: $\mathcal{L}_{\text{Reward-DPS}} \leftarrow \|\tilde{\epsilon}_\theta(x_t, t) - \epsilon_\theta(x_t, t)\|_2^2$
- 8: $g_n \leftarrow \nabla_\theta \mathcal{L}_{\text{Reward-DPS}}$
- 9: **end for**
- 10: $g \leftarrow \frac{1}{N} \sum_{n=1}^N g_n / \|g_n\|_2$
- 11: **return** g

F Additional Results

F.1 Local Concept Attribution

In this subsection, we present qualitative results for local concept attribution, which measures the contribution of training samples to specific concept manifestations that appear in generated images, rather than general concept contributions discussed previously. Figure 8 provides a qualitative comparison between global and local concept attribution results across several common concepts.

As shown in Figure 8(a), global concept attribution retrieves training samples that show diverse variations within each concept category, reflecting the broad range of examples that contributed to learning the general concept. In contrast, Figure 8(b) demonstrates that local concept attribution retrieves images that are considerably more similar to the specific concept manifestation in the generated image.

For example, in the “person” category, local attribution specifically retrieves male individuals matching the generated image, rather than a diverse mix of people. For “dog,” it retrieves bulldogs that closely resemble the specific breed shown in the generated image. Similarly, for “car,” it retrieves sports cars that match the style of the generated vehicle, and for “bird,” our method retrieves relatively subdued, gray-toned birds that correspond to the specific bird characteristics in the generated image.

This targeted retrieval demonstrates the effectiveness of local concept attribution in identifying training samples that contributed to specific visual and stylistic features, rather than just the general semantic category.

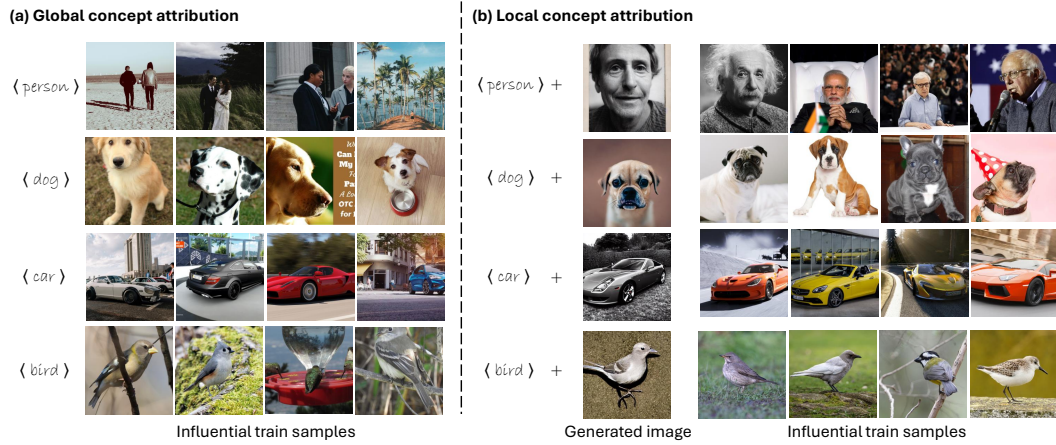


Figure 8: Comparison between global and local concept attribution. (a) Global concept attribution identifies training samples that contributed to learning general concepts (e.g., "person", "dog", "car", "bird") across all possible generations. The retrieved samples show diverse variations within each concept category. (b) Local concept attribution identifies training samples that specifically influenced the generation of particular instances of concepts in a given generated image. For each concept, we show a specific generated instance (left) and the most influential training samples (right) that contributed to that particular manifestation. Local attribution provides more targeted results, retrieving samples that closely match the specific visual characteristics, style, and context of the generated instance rather than the general concept category.